Catalysis Today 154 (2010) 118–126

Contents lists available at ScienceDirect

Catalysis Today

journal homepage: www.elsevier.com/locate/cattod

A novel mechanism for spectator CO-mediated reaction with unique *cis*-$(NO)_2$ dimer on a Co^{2+}-dimer/γ-Al_2O_3(1 1 0) model catalyst: Density functional theory calculations

Toshiaki Taniike[a,1], Mizuki Tada[a,2], Rudy Coquet[a], Yoshitada Morikawa[b], Takehiko Sasaki[c], Yasuhiro Iwasawa[a,*]

[a] Department of Chemistry, Graduate School of Science, The University of Tokyo, 7-3-1 Hongo, Bunkyo-ku, Tokyo 113-0033, Japan
[b] The Institute of Scientific and Industrial Research, Osaka University, Mihogaoka, Ibaraki, Osaka 567-0047, Japan
[c] Department of Chemistry, Graduate School of Frontier Science, The University of Tokyo, Kashiwanoha, Kashiwa, Chiba 277-8561, Japan

ARTICLE INFO

Article history:
Available online 8 April 2010

Keywords:
Density functional theory calculation
γ-Al_2O_3(1 1 0) surface structure
Supported Co catalyst
NO adsorption
cis-$(NO)_2$ dimer
Spectator CO
NO–CO reaction
Reaction mechanism

ABSTRACT

Density functional theory calculations for NO adsorption and NO–CO reaction on a Co^{2+}-dimer/γ-Al_2O_3(1 1 0) model catalyst were conducted to understand two new aspects of the increases in the amount and reduction rate of adsorbed NO by gas phase CO molecules which are undetectable at the Co^{2+}-ensemble/γ-Al_2O_3 catalyst surface. Three kinds of dinitrosyl adsorbates were found and assigned to normal *gem*-dinitrosyl species (*gem*-dinitosyl I and II) and an unique *cis*-$(NO)_2$ dimeric species. The *gem*-dinitrosyl II with a reconstructed structure involving Co–O_{surf} cleavage was considered as stable species experimentally observed, which is responsible for the spectator CO-promoted NO adsorption. We also found that the *cis*-$(NO)_2$ dimeric species specific for the Co^{2+}-ensemble structure possesses a much higher reactivity than the *gem*-dinitrosyl species, enabling the facile reaction with CO that is very weakly trapped at the surface. In the *cis*-$(NO)_2$ dimeric species two adsorbed NO molecules on two adjacent Co^{2+} sites interact with each other due to the opposed orientation of the unoccupied *d* orbitals of the two Co^{2+}, resulting in easy formation of a N–N bond through the $2\pi^*$–$2\pi^*$ hybridization. The NO adsorbates modify and activate the surface (Co^{2+} sites) to make pseudo-compounds (intermediates) with CO at the Co^{2+} sites in such a way that CO is not detected at the surface. The potential energy surface for the NO–CO reaction is presented and the transition states and intermediates are discussed.

1. Introduction

Ensemble catalysts with concerted metal ion sites often exhibit characteristic catalysis, which may not be performed by a single metal site [1–11]. We found a new phenomenon that the catalytic reduction and adsorption of NO on a Co^{2+}-ensemble/γ-Al_2O_3 catalyst were significantly promoted by gas phase CO undetectable at the catalyst surface [7,12–15]. The Co^{2+}-ensemble/γ-Al_2O_3 catalyst was prepared by chemical vapor deposition (CVD) of $Co_2(CO)_8$ on γ-Al_2O_3, followed by step-by-step treatments in a controllable manner, and characterized by EXAFS, diffuse reflectance UV/vis, FT-IR, Raman, TPD, etc [15–17]. The CVD Co^{2+}-ensemble/γ-Al_2O_3 catalyst thus obtained was *ca.* 50 times more active for $2NO + CO \rightarrow N_2O + CO_2$ than a usual impregnated Co^{2+}/γ-Al_2O_3 catalyst. The new aspect "surface catalytic reaction and adsorption assisted by gas phase molecules" is briefly summarized as follows. NO adsorbs to give paired peaks at 1769 and 1849 cm^{-1}, which may be considered as a *gem*-dinitrosyl species ($Co^{2+}(NO)_2$), while CO stays on the surface as shortly as *ca.* 10^{-10} s and its adsorbed amount is so small as undetectable volumetrically and IR-spectroscopically below their detection limits. Most of heterogeneous catalytic reactions are known to follow the Langmuir–Hinshelwood (LH) mechanism requiring the adsorption-mediated activation of reactant molecules rather than the Eley–Rideal (ER) mechanism which is induced by the collisional energy of impinging molecules from the gas phase. However, CO which rarely resides on the catalyst surface significantly promotes the reactivity of adsorbed NO to produce N_2O according to TPD of adsorbed NO. Further, the presence of CO in the gas phase also increases the equilibrium amount of NO adsorbed at the surface by

* Corresponding author. Present address: Department of Applied Physics and Chemistry, The University of Electro-Communications, Chofu, Tokyo 182-8585, Japan. Tel.: +81 42 443 5921; fax: +81 42 443 5483.
E-mail addresses: iwasawa@pc.uec.ac.jp, iwasawa@chem.s.u-tokyo.ac.jp (Y. Iwasawa).
[1] Present address: School of Materials Science, Japan Advanced Institute of Science and Technology, Nomi, Ishikawa 923-1292, Japan.
[2] Present address: Institute for Molecular Science, Myodaiji, Okazaki 444-8585, Japan.

0920-5861/$ – see front matter © 2010 Elsevier B.V. All rights reserved.
doi:10.1016/j.cattod.2010.03.048

ca. 2 times. Interestingly, a Co^{2+}-monomer/γ-Al_2O_3 catalyst prepared in a similar way to the Co^{2+}-ensemble/γ-Al_2O_3 catalyst had no activity for the same reaction and never showed the spectator CO-promoted NO adsorption, in spite of the similarity in the electronic state and local structure of their Co^{2+} sites [15]. Thus, the new surface phenomenon promoted by gas-phase CO molecules may originate from the Co^{2+}-ensemble structure. Importance of a synergistic cooperation between nearby Co^{2+} sites was also indicated to enhance the catalytic activity of the selective NO reduction on Co^{2+}/ferrierite catalysts [18,19]. However, it is hard to find experimentally the key issue and detailed mechanism for the surface event assisted by gas phase molecules because CO is neither spectroscopically nor volumetrically detectable at the surface under the reaction conditions.

Recently, we proposed a surface structure of a Co^{2+}-dimer/γ-Al_2O_3(1 1 0) model catalyst based on the experimental characterizations and density functional theory (DFT) calculations [20], and suggested that an adsorbate–adsorbate interaction imposed by the opposed orientation of the unoccupied *d* orbitals of the adjacent Co^{2+} ions may be the origin of the new catalytic phenomenon on the Co^{2+}-ensemble catalyst [15,21]. By means of the DFT calculations closely compared with our recent experimental results [15], here we report that a *cis*-$(NO)_2$ dimeric species through the adsorbate–adsorbate interaction is the origin of the high activity of the Co^{2+}-ensemble/γ-Al_2O_3 catalyst, and that this highly reactive *cis*-$(NO)_2$ dimer enables the reaction with only weakly adsorbed, namely chemically unactivated CO molecules. We also suggest that the CO-promoted NO adsorption may be correlated with the appearance of a new *gem*-dinitrosyl species accompanied with CO-induced cleavage of a Co–O_{surf} bond at the interface.

2. Calculation

The density functional theory (DFT) at the level of generalized gradient approximation (GGA) [22] has been employed throughout calculations. The exchange–correlation functional was of Perdew–Burke–Ernzerhof (PBE) [23]. The basis set was the double numeric basis with polarization functions (DNP) [24], whose accuracy is comparable to the famous 6-31G** basis. The core parts were described by the effective core potentials (ECP) of Dolg et al. [25,26]. These calculations were conducted by the DMOL3 program package [24]. The catalyst surface was modeled by a repeated slab separated by a *ca*. 1-nm vacuum region. The *k*-point mesh was $3 \times 4 \times 1$ (the size of the unit cell was 0.79110, 0.55939 and 1.90503 nm, which had been decided in the previous calculations [20]). The convergence criterion for SCF calculations was 1.0×10^{-5} Hartree and those for geometry optimization were 2.0×10^{-5} Hartree in energy and 2.1×10^{-3} Hartree/Bohr in force.

The vibrational frequencies of adsorbates were calculated in a way that force constants, second-order derivatives of energy were approximated by a numerical differentiation, where each atom was displaced from the equilibrium position by 0.001 nm in the *x*, *y*, and *z* directions. In addition, we used a partial hessian consisting of the force constants of a Co^{2+} dimer and adsorbates, which accurately reproduced the vibrational frequencies obtained by diagonalizing a total hessian.

Transition state searches were executed as follows. At first, the linear synchronous transit method (LST) [27] was used to search the energy maximum in the line connecting a reactant and product. From this approximate energy maximum, energy minimization in the direction conjugate to the reaction pathway (CG) was conducted. Then the quadratic synchronous transit method (QST) was used to improve the energy maximum point. Finally the CG/QST cycle was repeated until the gradient at the transition state decreased within 5.3×10^{-3} Hartree/Bohr. The obtained transition state was refined in order to give a sole imaginary frequency for the reaction coordinate. Further, we confirmed whether the obtained transition state corresponded to the maximum in the reaction pathway or not by additional LST/QST/CG calculations between the reactant (product) and the transition state.

As was described in the previous calculations [20], each Co^{2+} ion had a high spin state, i.e. $Co^{2+}(\uparrow\uparrow\uparrow)$ and the relative spin orientation of the adjacent Co^{2+} ions ($Co^{2+}(\uparrow\uparrow\uparrow)\cdots Co^{2+}(\uparrow\uparrow\uparrow)$ or $Co^{2+}(\uparrow\uparrow\uparrow)\cdots Co^{2+}(\downarrow\downarrow\downarrow)$) did not affect the energy and structure of the catalyst model. Because CO does not have any unpaired electron, CO adsorption was totally independent of the spin orientation of the adjacent Co^{2+} ions. NO with one unpaired electron in a $2\pi^*$ orbital is known to makes its doublet anti-parallel to the spin of Co^{2+} ($Co^{2+}(\uparrow\uparrow\uparrow)$–NO($\downarrow$)) [28], and as for the relative preference we confirmed that the anti-parallel orientation was 0.25 eV more stable than the parallel orientation. In addition, bridging NO adsorbates, which emerged in mononitrosyl or geminal species as a result of the underestimated Co–N bond length (described later), always favored the $Co^{2+}(\uparrow\uparrow\uparrow)$–NO($\downarrow$)–$Co^{2+}(\uparrow\uparrow\uparrow)$ spin configuration than $Co^{2+}(\uparrow\uparrow\uparrow)$–NO($\downarrow$)–$Co^{2+}(\downarrow\downarrow\downarrow)$ by 0.2–0.3 eV. Therefore, we fixed the total spin at $6-x$ in a system which included *x* NO adsorbates (x = 0–2). Such restriction to the total spin density gives correct spin states on metal ions, compared to spin-unrestricted calculations [29].

In our calculations, a Co^{2+} dimer composed of the two adjacent Co^{2+} ions weakly interacted with each other significantly prevented a SCF cycle from converging because multiple *d* orbitals underlay in a narrow energy region. For this convergence problem, we employed the following scheme [20] using the thermal smearing method [30]. Firstly, a single-point calculation with a high smearing temperature, 0.010 Hartree was done. Next the obtained electronic state was re-converged with a milder smearing rate, 0.008 Hartree. In this way, the smearing rate was gradually decreased to 0.004 Hartree, which was enough small to evaluate accurate energies and frequencies (the error ranges which were derived from calculations about several dinitrosyl-Co^{2+} complexes, were 0.05–0.10 eV for the energy and 10–20 cm^{-1} for the frequency).

The interaction between NO and highly correlated metal or metal ions is one of the major challenges of DFT with pure functionals such as PBE. In our system, the adsorption energy of mononitrosyl species bridging the two adjacent Co^{2+} ions was overestimated as largely as by *ca*. 1.5 eV, and its vibrational frequency was greatly red-shifted by 180 cm^{-1}, indicating an overestimated back-donation from Co^{2+} to NO. Similar problems of the pure-functional DFT have been reported for CO adsorption on a Pd(1 1 1) surface [31,32], CO and NO adsorption on a strongly correlated NiO(1 1 0) surface [29,33,34], and so on. These problems partly come from the well-known fact that the pure-functional DFT underestimates the gap size between valence and conduction bands (or orbitals) [35]. The underestimation of the HOMO-LUMO gap size of NO in the pure-functional DFT results in an overestimated back-donation into the unoccupied $2\pi^*$ orbital of NO, which leads to the increase of adsorption energies, red-shift of the vibrational frequencies, and elongation of the N=O bond length. Since the degree of the error depends on the kind of the adsorption sites and the number of the metal ions bound to NO, we did not compare the relative stability of various NO adsorbates at different sites and adsorption modes. Another source of the problems is the incorrect description of the on-site Coulomb repulsion [29], which causes spin overmixing between a highly correlated metal ion and NO, i.e. shrinks and strengthens the Co^{2+}–N bond. In spite of these problems, however, it is known that the activation barrier for the N–O scission is much more accurate due to the error cancellation [36,37]. Similarly, we confirmed that the difference between the asymmetric and symmetric vibration frequencies of dinitrosyl

species was relatively accurate. Thus, we continuously employed the PBE functional for the NO–CO reaction.

On the other hand, we also conducted DFT+U calculations for the most important *cis*-$(NO)_2$ dimeric species to circumvent the spin overmixing problem using the program package of VASP [38], where the Dudarev type [39] was applied with U = 6.5 and J = 1 for the *d* electrons of Co^{2+} (parameters were decided to fit to the total magnetization of cobalt oxide). In this additional calculation, the PBE functional, projector-augmented wave (PAW) method [40], plane wave basis set with the kinetic-energy cutoff of 400 eV, and $3 \times 5 \times 1$ *k*-points were employed.

3. Results

3.1. Co^{2+}-dimer/γ-Al_2O_3 model catalyst

In this section, we briefly summarize the characteristics of the Co^{2+}-dimer/γ-Al_2O_3 model catalyst, which was derived in the previous DFT calculations [20]. A Co^{2+} dimer is believed to be an active unit for the NO–CO reaction ($2NO + CO \rightarrow N_2O + CO_2$) on the Co^{2+} ensemble/γ-Al_2O_3 catalyst prepared by $Co_2(CO)_8$ precursor, since EXAFS analysis gave the coordination number of 0.8 for the Co–Co bond of 0.33 nm [17] and the maximum coverage of NO was 2NO per Co^{2+} dimmer [15]. Among several tens of models which were obtained by supporting a Co^{2+} dimer on a γ-Al_2O_3(1 1 0) surface through the reaction with surface hydroxyl groups, the structure in Fig. 1 meets all the experimental results for the electronic and local structure of the Co^{2+} species [15,17]. In this model, Co^{2+} ions have a high spin state and are three-folded by O(II), O(III), and O(I)H (the Roman number in parentheses indicates the coordination number of O in terms of Al). The Co^{2+} ions are situated in a trigonally distorted T_d symmetry, which coincides with the previous UV and XANES results [15,17]. The averaged Co–O distance is 0.191 nm, which reproduces 0.193 nm determined by EXAFS [15]. The Co–Co distance, which is the most important issue of evaluation of the validity of the surface model, is 0.316 nm, which agrees with the EXAFS value, 0.33 nm [17].

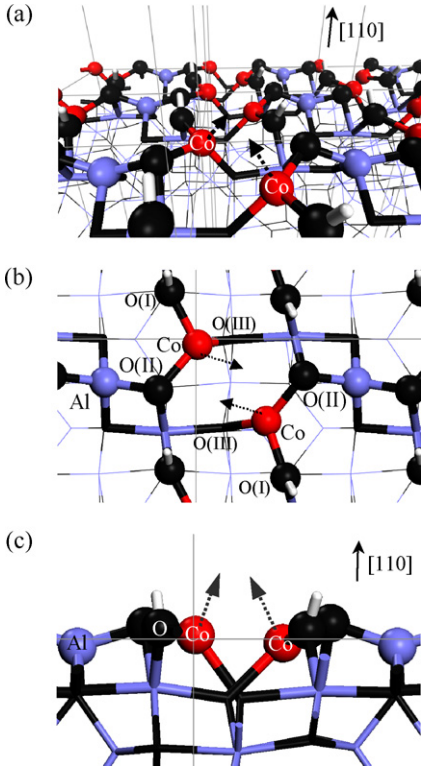

Fig. 1. (a) Perspective, (b) top, and (c) side views of the proposed Co^{2+}-dimer/γ-Al_2O_3 model catalyst surface. The coordination numbers of O around Co^{2+} are shown in terms of Al. The arrows indicate the orientation of unoccupied *d* orbitals of Co^{2+}. Black: O, pale purple: Al, red: Co, white: H.

As described in Section 1, the behavior of the Co^{2+}-ensemble catalyst is different from the Co^{2+} monomer catalyst only in the coexistence of spectator CO, i.e. the Co^{2+}-ensemble catalyst shows its ensemble aspect only in the limited situation. In the previous study [15,20,21], we suggested that the structural origin of these behaviors is the opposed orientation of the unoccupied *d* orbitals of the adjacent Co^{2+} ions, shown as arrows in Fig. 1. When one NO molecule adsorbed on the Co^{2+}-dimer catalyst and the Co^{2+}-monomer catalyst, the both Co^{2+} catalysts gave a very similar adsorption structure. However, when another NO molecule was added at the adjacent Co^{2+} site in the dimer catalyst, the co-adsorbed two molecules could interact with each other because of the special orientation of the Co^{2+} dimer. This adsorbate–adsorbate interaction was the most prominent character of our Co^{2+}-dimer/γ-Al_2O_3 model catalyst and we proposed that it should be the key to the NO adsorption and catalysis [20].

3.2. Possible dinitrosyl species

Starting from various initial structures, three different dinitrosyl species were finally obtained on the Co^{2+}-dimer model catalyst, shown in Fig. 2(a) and(c) [21]. Two of them in Fig. 2(a) and (b) are conventional geminal species (two NO molecules adsorb at one Co^{2+} ion), and they are denoted as *gem*-dinitrosyl I and II species, respectively. *gem*-Dinitrosyl adsorbates are a quite general species in organometallic complexes [41] and also on supported metal-ion catalysts [42–44]. The two *gem*-dinitrosyl species are different from each other in the extent of surface reconstruction around Co^{2+}: the *gem*-dinitrosyl I accompanied little reconstruction, while the formation of the *gem*-dinitrosyl II required the scission of the Co–O(III) bond (the Co–O length changes from the original Co–O(III) length of 0.217–0.373 nm). The other stable species was a *cis*-$(NO)_2$ dimeric species, where the two N atoms at the adjacent Co^{2+} sites faced to each other with the terminating O atoms in the reversed direction (Fig. 2(c)) [15,21]. It is notable that the two NO molecules couple with each other through an adsorbate–adsorbate interaction, which is the most prominent feature of the Co^{2+}-dimer catalyst [20]. Although similar species have been observed in gas-phase [45,46] and they have also been proposed based on DFT calculations on the Ag(1 1 1) [47,48], Pt(2 1 1) [49], and Rh surfaces [50], to our knowledge it is the first to report the *cis*-$(NO)_2$ dimeric species on the supported metal/metal ion catalysts. The dimerization of NO in the gas phase is still a difficult system for the DFT calculations [51], but the *cis*-$(NO)_2$ dimer on the Co^{2+}-dimer model catalyst was much easier to be described by the DFT because the alignment of the Co^{2+} dimer required the dimerization of NO. Namely, the formation of the *cis*-$(NO)_2$ dimer was caused by the geometric feature of the Co^{2+} sites on the γ-Al_2O_3 surface, not by a weak and difficult spin coupling between two NO adsorbates. Considering that the experimentally obtained N–N distance of the gas-phase dimer was between 0.175 and 0.233 nm [45,46] and that on the Ag(1 1 1) surface was 0.15 nm [48], our *cis*-$(NO)_2$ dimer had relatively larger N–N length of 0.251 nm, which was both due to the large Co–Co distance of 0.317 nm and to the underestimated Co–N length by the pure-functional DFT. In the present study we conducted additional DFT+U optimization. The DFT+U calculation indicated a decrease of the N–N length from 0.251 to 0.176 nm accompanied with enlarging the Co–N distance from 0.183 to 0.205 nm (Fig. 2(d)), which implies the easier formation of the N–N bond to lead to N_2O product.

The adsorption properties of the three species are summarized in Tables 1 and 2. The *cis*-$(NO)_2$ dimeric species looked the most sta-

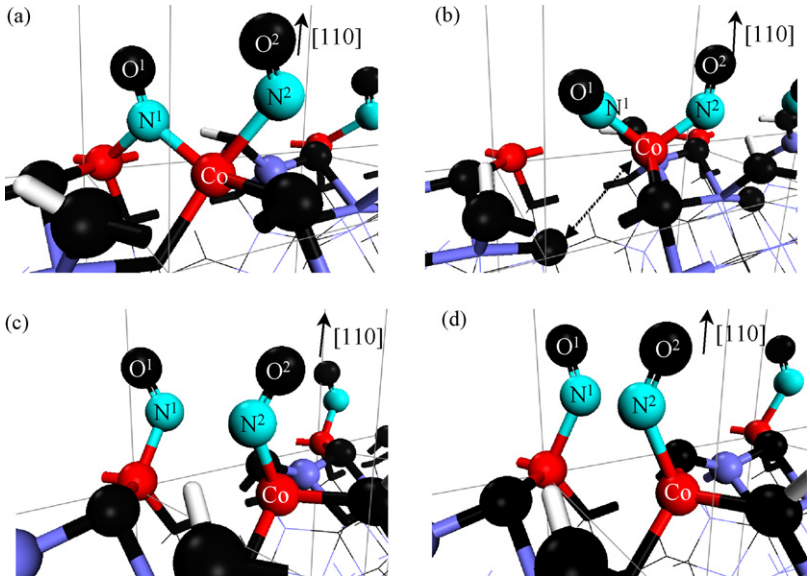

Fig. 2. Possible adsorption states of dinitrosyl species: (a) *gem*-dinitrosyl I, (b) *gem*-dinitrosyl II, and (c) *cis*-$(NO)_2$ dimeric species optimized by DFT, and (d) *cis*-$(NO)_2$ dimeric species re-optimized using DFT+U. The arrow in (b) indicates the scission of the Co–O(III) bond. Black: O, pale purple: Al, red: Co, gray: C, light blue: N, white: H. This color scheme is kept in subsequent Figures.

Table 1
Adsorption energies and vibrational frequencies of mononitrosyl and dinitrosyl adsorbates.

Species[a]	E_{ad}/eV		Frequency/cm^{-1}	
	Calc.	Exp.	Calc.[c]	Exp.
Mononitrosyl	−1.78	≤0.3	1643	1823
gem-Dinitrosyl I	−1.89		1624, 1768	1769, 1849
gem-Dinitrosyl II	−2.28	−0.61	1656, 1767	
cis-$(NO)_2$ dimer	−2.71	(−0.78)[b]	1613, 1729	
cis-$(NO)_2$ dimer (DFT+U)	−1.69		n/a	

[a] The corresponding species are shown in Fig. 2.
[b] The parenthetic value is the adsorption energy of the more stable 2NO, which was produced by coexistence of CO.
[c] The vibrational frequency of NO(g) was calculated as 1889 cm^{-1}.

ble, apparently because of the overestimated back-donation from the two Co^{2+} ions to NO. On the one hand, the *gem*-dinitrosyl II was *ca.* 0.4 eV more stable than the *gem*-dinitrosyl I in spite of the fact that the bridged NO in the *gem*-dinitrosyl I took extra back-donation (see also that the frequencies of the *gem*-dinitrosyl I were red-shifted more than those of the *gem*-dinitrosyl II). Namely, the energy difference between the geminal I and II must be meaningful, referring to the problems of the pure-functional DFT. The averaged frequencies between the symmetric and asymmetric modes were 1696 cm^{-1} for the geminal I, 1711 cm^{-1} for the geminal II, and 1672 cm^{-1} for the *cis*-$(NO)_2$ dimer, thus all of which were significantly red-shifted compared to the IR result, average 1809 cm^{-1} due to the problems of the pure-functional DFT. As mentioned above, the amount of the red-shift largely depends on the mode of adsorption and the number of the involved Co^{2+} ions, and therefore the comparison of the averaged frequencies among the different species is meaningless. Instead we focused on the splitting of the paired frequencies of the three adsorbates. The two conventional *gem*-dinitrosyl species showed the splitting over 100 cm^{-1}, and surprisingly the frequencies of the *cis*-$(NO)_2$ dimeric species split into 1613 and 1729 cm^{-1} like those of the *gem*-dinitrosyl species, rather than that of two mononitrosyl species. This finding proves the existence of a coupling between the two NO adsorbates in the *cis*-$(NO)_2$ dimeric species, and the compatibility of the *cis*-$(NO)_2$ dimer with the appearance of asymmetric and symmetric stretching peaks in FT-IR spectra [15]. Indeed, the normal modes of 1613 and 1729 cm^{-1} behaved equally to asymmetric and symmetric stretching vibrations of a *gem*-dinitrosyl species where the coupling center for the *cis*-$(NO)_2$ dimeric species is virtually positioned at the intermediate position between the adjacent Co^{2+} sites.

Table 2
Structural parameters of mononitrosyl and dinitrosyl adsorbates.

Species	Distance[a]/nm			
	Co–N^1	Co–N^2	N^1–O^1	N^2–O^2
Mononitrosyl	0.194, 0.194	–	0.1195	–
gem-Dinitrosyl I	0.189, 0.204	0.210	0.1192	0.1167
gem-Dinitrosyl II	0.177	0.174	0.1183	0.1175
cis-$(NO)_2$ dimer	0.182	0.184	0.1185	0.1185
cis-$(NO)_2$ dimer (DFT+U)	0.203	0.207	0.1193	0.1193

[a] The numbers on atoms correspond to those in Fig. 2. The calculated bond length of NO(g) was 0.1164 nm.

3.3. Reaction mechanism

Next, we examined possible reaction mechanisms between the three types of dinitrosyl species and CO. Prior to the reaction between the dinitrosyl species and CO, the possibility of the two-step reaction mechanism, $2NO \rightarrow N_2O + O_{ad}$ and $O_{ad} + CO \rightarrow CO_2$, was checked. Though the experimental results excluded this mechanism, two Co^{2+} sites might be sufficient to dissociate NO to form atomic N and O adsorbates. At first, the bridged mononitrosyl species was tilted to make a Co^{2+}–N=O–Co^{2+} structure, which required only 0.15 eV energetic penalty. However, when the N–O bond length of the tilted NO was manually elongated from 0.122 to 0.17 and to 0.22 nm, the energy increased by 0.47 and 2.16 eV, respectively. Thus the energy of the tilted NO monotonically increased towards the dissociation because of the extreme instability of the atomic adsorbates. Finally we excluded the two-step pathway, consistently with the experiments.

From the geminal species I, two reaction pathways were found, whose transition states were denoted as TS 1 and TS 2 (see Ref. [21] for the details). The activation energy for the ER mechanism was as large as 2.49 eV, because the Co–N–Co–N=O intermediate species was 2.36 eV less stable than a N_2O(g) molecule. The acti-

Table 3
Structural parameters of the transition and intermediate states.

Structure[a]	N^1–O^1/nm	O^1–C/nm	C–O^2/nm	N^1–N^2/nm	Co–C/nm
TS 3-1	0.1339	0.1790	0.1159	0.1322	–
Int 3	0.1451	0.1381	0.1191	0.1293	–
TS 3-2	0.1654	0.1291	0.1207	0.1264	–
TS 4-1	0.1285	0.2004	0.1155	0.1351	0.2199
Int 4	0.1482	0.1368	0.1206	0.1287	0.1945
TS 4-2	0.1811	0.1294	0.1223	0.1220	0.2018

[a] The corresponding transition and intermediate states are in Fig. 3.

vation energy for the LH mechanism was also as large as 1.66 eV though the value was smaller than that for the ER mechanism. This was because the transition state of the LH pathway was relatively near the product side, and therefore a part of the heat of CO_2 formation contributed to the stabilization of the transition state. The reactivity of the *gem*-dinitrosyl II with CO was obviously much less than that of the *gem*-dinitrosyl I due to its quite large Co–Co distance, which prevented both the ER and LH mechanisms.

For the reaction between the *cis*-$(NO)_2$ dimer and CO, ER and LH pathways were found, denoted as paths (a) and (b) in Fig. 3, respectively. Both of them were composed by two elemental steps: the N–N formation and subsequent N–O bond cleavage. In the ER path (a), a CO(g) molecule approached either of NO directly from the gas phase with its molecular axis nearly vertical to the surface. At the first transition state (TS 3-1), the N^1–N^2 distance decreased to 0.132 nm by utilizing the collisional energy of the CO molecule (Table 3). After a shallow intermediate state (Int 3), the N^1–O^1 was cleaved to make CO_2 at the second transition state (TS 3-2). The heights of the TS 3-1 and TS 3-2 from the reactant were 1.13 and 0.88 eV, respectively. In the LH path (b), a CO molecule very weakly trapped at one Co^{2+} induced the shrink of the N^1–N^2 distance to 0.135 nm at the first transition state (TS 4-1, Table 3). The interaction between the CO molecules and the Co^{2+} ion was slightly endothermic (*ca.* 0.2 eV) at the reactant, consistently with the experimental absence of CO on the surface. However, the interaction gradually varied to attractive one toward the TS 4-1, resulting in the stabilization of the TS 4-1, whose height from the reactants was 1.07 eV. After surpassing the TS 4-1, a stable surface complex (Int 4) was formed among the CO, 2NO and Co^{2+} dimer, where the attractive CO–Co^{2+} interaction significantly contributed the stabilization. Finally at the TS 4-2, the stable complex begun to form CO_2 with a very small activation barrier, and the N^1–N^2 distance was further decreased to 0.122 nm. It is likely that CO molecules physically trapped by the catalyst surface migrate to a Co^{2+} site having the *cis*-$(NO)_2$ dimer, and then react only in the case that the *cis*-$(NO)_2$ dimer has a sufficient internal energy to surpass the TS 4-1. The heat of the formation of Int 4 is readily available to overcome the small barrier at TS 4-2, and therefore the reaction never stays at Int 4 for a detectable time. In the both paths, the common product state of the bridging N_2O adsorbate, whose energy was only 0.18 eV less stable than that of N_2O(g), easily desorbed from the catalyst surface without any notable barrier. It is also noteworthy that the N–N bond formation provides the stable surface pseudo-compound intermediates with gaseous or weakly trapped CO in both the paths.

4. Discussion

4.1. Relationship between theoretical and experimental results

To discuss on the dinitrosyl species and NO–CO reaction mechanism, let us briefly summarize our experimental findings on the Co^{2+}-ensemble/γ-Al_2O_3 catalyst [15].

(i) At least two kinds of dinitrosyl species on the Co^{2+}-ensemble/γ-Al_2O_3 catalyst were found: species A produced in the absence of gaseous CO and species B produced only in the presence of CO(g). In the absence of CO (g), NO adsorbed on the catalyst as species A; for example, the adsorbed amount was typically 0.18 NO molecule per Co under 5.3 kPa of NO pressure at 443 K. The adsorption energy was decided as 59 kJ/mol (0.61 eV), and the vibrational frequencies for the adsorbed NO were 1769 and 1849 cm^{-1}, which had been assigned to asymmetric and symmetry stretching modes of *gem*-dinitrosyl species, respectively.

(ii) The presence of spectator CO in the gas phase drastically enhanced the equilibrium adsorption amount from 0.18 to 0.35 NO per Co, where the species A and B coexisted on the catalyst surface. The newly generated species B was responsible for the increase in the equilibrium adsorption amount. The species B was 16 kJ/mol more stable than the species A, while its vibrational frequencies were almost the same to those of the species A, and consequently the species B was considered as *gem*-dinitrosyl species.

(iii) The transformation from the species A to B required the activation energy of 86 kJ/mol in the presence of CO, and that of the backward transformation from the species B to A was as large as 159 kJ/mol in the absence of CO. Actually the species A was readily removed from the catalyst surface by evacuation, but the species B remained sticking on the catalyst surface under vacuum. When NO(g) was re-admitted after evacuation of the pre-exposed surface, the species A recovered, and the species B still remained on the surface in spite of the absence of CO(g) and of the frequent exchange between NO_{ad} and NO(g), which suggested that the promoting effect of CO was memorized on the catalyst surface structure. Thus, it can be inferred that the generation of the species B require some surface reconstruction, whose barrier becomes accessible only in the presence of CO(g).

(iv) In addition to the enhanced NO adsorption, CO(g) significantly proceeded the reaction $2NO + CO \rightarrow N_2O + CO_2$ on the Co^{2+}-ensemble/γ-Al_2O_3 catalyst, whose activity was *ca.* 50 times higher than that of an impregnated Co^{2+}/γ-Al_2O_3 catalyst. On the other hand, the Co^{2+}-monomer/γ-Al_2O_3 catalyst prepared similarly to the Co^{2+}-ensemble catalyst showed no activity for the same reaction under the similar reaction conditions. This suggests that the reaction mechanism should result from the ensemble structure. A set of temperature programmed reactions revealed that only the species A contributed to the activity of the Co^{2+}-ensemble catalyst, while the species B was hard to react with CO(g). The activation energy for the reaction was 0.74 eV from the energy of the species A.

Based on the DFT calculations on the Co^{2+}-dimer/γ-Al_2O_3 model catalyst surface, three dinitrosyl species were suggested: *gem*-dinitrosyl I and II, and *cis*-$(NO)_2$ dimeric species as shown in Fig. 2. The *gem*-dinitrosyl I and *cis*-$(NO)_2$ dimer without any notable reconstruction of the catalytic surface seemed to be easily formed without CO. Namely, both of them or either of them may correspond to the species A that is highly reactive to CO. On the other hand, the formation of *gem*-dinitrosyl II required to surpass a barrier for the Co–O(III) bond scission. In addition, the *gem*-dinitrosyl II had little reactivity with CO as was described in Section 3.3. It is most plausible from these facts that the *gem*-dinitrosyl II is the species B, and the CO effect on the increase of the adsorbed NO amount may be memorized through the Co–O(III) bond scission. However, we could not discuss the effect of spectator CO on the barrier of the bond scission, due to the large error range of the pure-functional DFT.

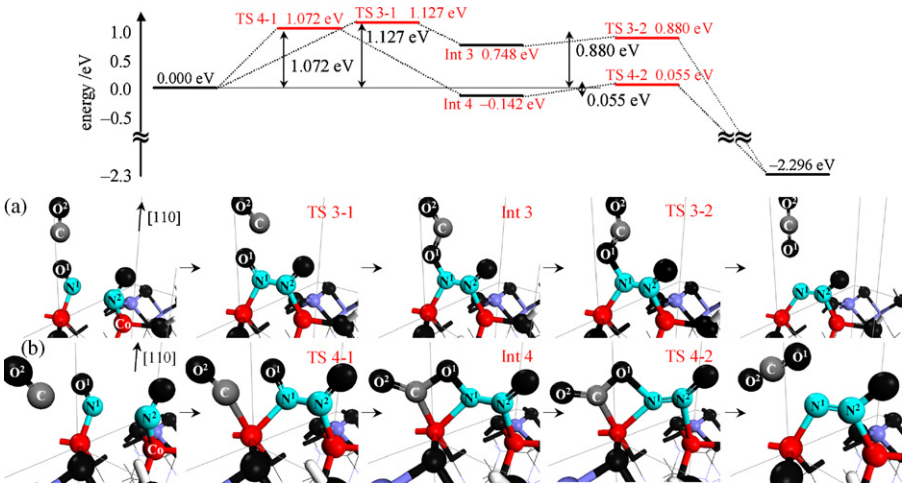

Fig. 3. Possible reaction pathways between *cis*-$(NO)_2$ dimer and CO to produce $N_2O + CO_2$. Path (a) of the Eley–Rideal type, where CO directly collides with the *cis*-$(NO)_2$ dimer, and path (b) of the Langmuir–Hinshelwood type, where CO is only weakly trapped by one Co^{2+} site. The progress of the reaction accompanies an attractive interaction between CO and Co^{2+} to stabilize the first transition state and intermediate state in the path (b).

Next, we simulated and compared the four mechanisms between the *gem*-dinitrosyl I or *cis*-$(NO)_2$ dimeric species and CO, and found that the *cis*-$(NO)_2$ dimeric species obviously had a much higher reactivity with CO than the *gem*-dinitrosyl species which is conventionally believed as reactive species [12–14,42,44]. This somewhat surprising trend must not be changed by more sophisticated calculations since the DFT+U suggested the easier formation of the N–N bond (a rate-limiting step in the paths (a) and (b) of Fig. 3) by elongating the N–Co^{2+} distance. Furthermore, the pure-functional DFT calculations are known to be accurate in energy barrier for the N–O bond breaking [36,37]. Thus, we concluded that the highly reactive species is the *cis*-$(NO)_2$ dimeric species, whose vibrational frequencies were compatible with the IR, and that the species A corresponds to the *cis*-$(NO)_2$ dimeric species or to a mixture of the *cis*-$(NO)_2$ dimer and the *gem*-dinitrosyl I. The proposed reaction mechanisms between the *cis*-$(NO)_2$ dimer and CO (the paths (a) and (b) in Fig. 3) had similar activation barriers at the rate-limiting steps, *ca.* 1.1 eV, which are acceptable compared to the experimental value, 0.74 eV [15]. In addition, both the paths meet the above-mentioned prerequisite: the reaction with gaseous or very weakly trapped CO molecules and particular to the Co^{2+} dimeric structure as the *cis*-$(NO)_2$ dimeric species itself is specific for the Co^{2+} dimer. However, as in the great majority of surface-catalyzed reactions, the LH path (b) is entropically much more advantageous than the ER path (a). In the path (4), CO migrates to a Co^{2+} site without a strong chemical interaction at the reactant, while it starts to chemically interact with the Co^{2+} site at the transition state. This mechanism provides a new aspect of catalysis to understand how the active site contributes to the activation of a reactant to promote its reaction even if the reactant has almost no interaction/adsorption with the active site at the static state. CO adsorption on the Co^{2+} dimer is undetectable, but the NO adsorbates modify the active Co^{2+} sites on the surface and the new surface adsorbs CO but in such a way that it cannot be detected.

4.2. The origin of the high reactivity of the cis-$(NO)_2$ dimer to CO

Here a detailed analysis is conducted to uncover the origin of the high reactivity of the *cis*-$(NO)_2$ dimer with CO. First, the C–O^1 distance in the path (a) of Fig. 3 was manually varied from the reactant to the TS 3-1 to see the change in the N^1–N^2 distance (Fig. 4(a)). When the C–O^1 distance was larger than 0.22 nm, the N–N distance remained almost unchanged at the same distance as that of the reactant. The further approach of the CO molecule shortened the N–N distance, and led to the N–N bond formation, and finally the N–N distance became to 0.132 nm at the transition state (Fig. 4 and Table 3). Also in the path (b) of Fig. 3, the shrink of the Co–C distance shortened the N–N distance to 0.135 nm at the TS 4-1 (Table 3). Activation energies in the both pathways were *ca.* 1.1 eV similarly to each other.

Then, it was examined why the CO molecule that adsorbs very weakly at an undetectable level can make the N–N bond with the energetic penalty of only 1.1 eV. In order to answer this question, the energy was plotted by changing the N–N distance without CO. In Fig. 4(b), it was found that the energetic penalty to make the N–N bond was even smaller than 1.1 eV in the case of the presence of CO. Jigato et al. [47] performed a similar DFT simulation for

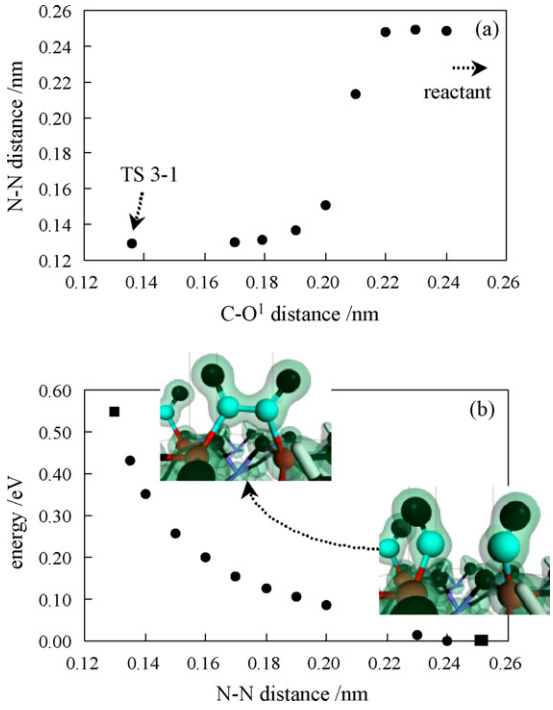

Fig. 4. (a) Evolution of the N–N distance in terms of the C–O^1 distance in the path (a) of Fig. 3. (b) Energy change in decreasing the N–N distance without CO, where the electron densities in the insets indicate the formation of the covalent N–N bond at *ca.* 0.135 nm of the N–N distance.

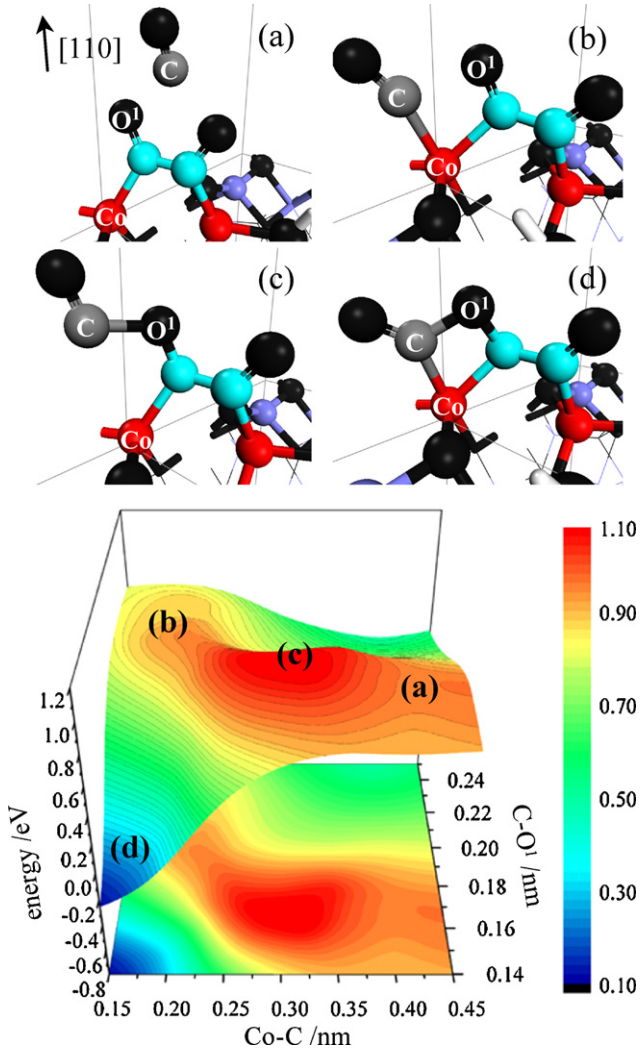

Fig. 5. The potential energy surface (PES) around the TS 3-1 and TS 4-1. The C–O^1 and Co^{2+}–C distances are scanned, while fixing the N–N distance at 0.135 nm, to examine the connectivity between the paths (a) and (b). Some representative structures in the potential energy surface are also shown in (a)–(d).

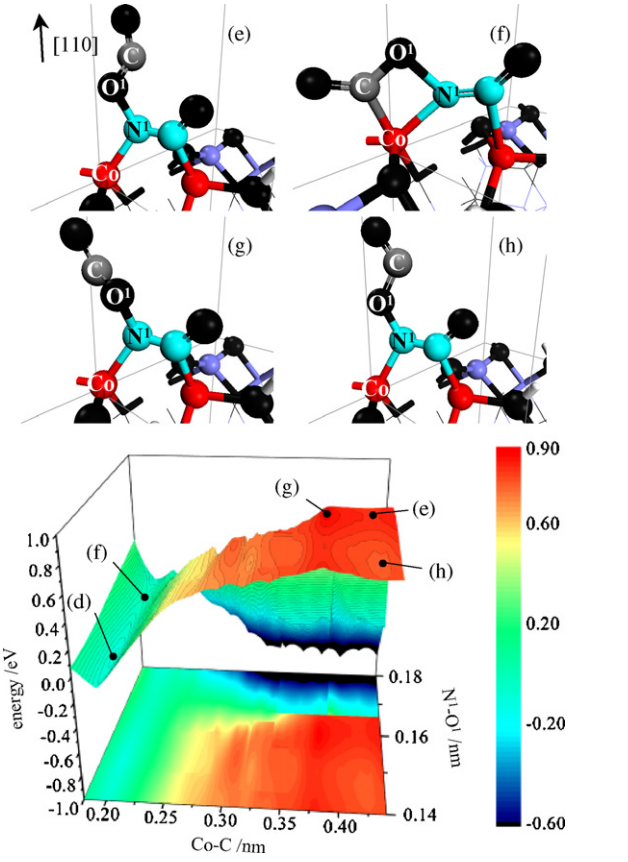

Fig. 6. The potential energy surface (PES) around the TS 3-2 and TS 4-2. The N^1–O^1 and Co^{2+}–C distances are scanned with the N–N distance optimized. Again, representative structures in the PES are shown in (e)–(h). Note that the point (d) coincides with that in Fig. 5, and the point (e) is connected to the point (a) in Fig. 5.

the formation of a *cis*-$(NO)_2$ dimeric species on a Ag(1 1 1) surface. They reported the disappearance of the spin densities of the NO molecules (from the doublet) after the dimer formation and such a delocalization of the unpaired electrons of NO was due to the $2\pi^*$–$2\pi^*$ bonding between the two NO molecules. When the N–N distance of our *cis*-$(NO)_2$ dimeric species decreased from 0.251 to 0.190 and to 0.135 nm, the Mulliken spin density on the N atoms decreased to 0.26 and 0.11, respectively, from the original spin density, 0.41. This is an evidence for the formation of the $2\pi^*$–$2\pi^*$ bonding between the two NO molecules. This is also supported by the change in the electron density shown in the insets of Fig. 4(b). Consequently, we showed that the relatively small activation energies in the paths (a) and (b) of Fig. 3 were caused by the ease of the N–N bond formation of the *cis*-$(NO)_2$ dimeric species through the $2\pi^*$–$2\pi^*$ hybridization, and that the significant activity of the Co^{2+}-ensemble/γ-Al_2O_3 catalyst for the NO–CO reaction was attributed to the property of the *cis*-$(NO)_2$ dimeric species on the Co^{2+} dimer with the opposed orientation of the unoccupied orbitals. On the other hand, the complete inertness of the Co^{2+} monomer catalyst must be owing to the lack of this species. Thus, it is suggested that such a special configuration of supported metal ions can dramatically promote the NO reaction even with inert molecules that weakly adsorb or undetectable at the catalyst surface.

4.3. Relationship between paths (a) and (b)

The paths (a) and (b) of Fig. 3 for the NO–CO reaction on the Co^{2+}-dimer/γ-Al_2O_3 model catalyst have an important common feature: the N–N distance decreased to 0.132–0.135 nm at the rate-limiting step with the similar energetic penalty of *ca.* 1.1 eV (Table 3). On the other hand, the major difference between the TS 3-1 and TS 4-1 is the reaction coordinates: the C–O^1 distance in the path (a) and the Co^{2+}–C distance in the path (b). To examine the connectivity between the two paths, a two dimensional potential energy surface (PES) was drawn by manually scanning the C–O^1 and Co^{2+}–C distances around the TS 3-1 and TS 4-1, while fixing the N–N distance at 0.135 nm (Fig. 5). The employed grid size in the manual scan was 0.01 nm for the energetically important regions around the points (a)–(d), while the other less important regions were plotted with thinner grids. The points (a) and (b) nearly correspond to the TS 3-1 and TS 4-1, respectively. The heights of these points are *ca.* 1.0 eV (slight structural deviations from the real transition states decreased the energies by about 0.1 eV). The point (d) is near the Int 4 of the path (b) (Fig. 3). When the ridge line from the points (a) and (b) was traced, the maximum was found at the point (c), where CO approaches to one NO sideways. Notablly the point (c) was only *ca.* 0.2 eV higher than the points (a) and (b), which indicates that the TS 3-1 in the path (a) and TS 4-1 in the path (b) are rather continuous at the reaction temperature 333–463 K. This continuity of the PES again proved the high reactivity of the *cis*-$(NO)_2$ dimer even with gaseous or very weakly trapped CO molecules, both of which were not activated by chemisorption. However, the reaction

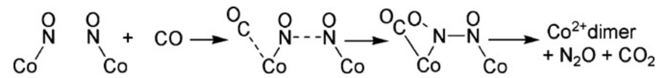

Scheme 1. The most plausible mechanism for $2NO + CO \rightarrow N_2O + CO_2$ on the Co^{2+}-dimer/γ-Al_2O_3 catalyst.

dominantly proceeds along the LH path (b) in an entropic reason at a finite temperature, even though the two pathways have similar activation energies.

A similar two-dimensional PES was drawn for the latter part of the reaction with respect to the Co^{2+}–C and N^1–O^1 distances (Fig. 6). The employed grid densities for the two coordinates were similar to those in Fig. 5, while the N–N distance was allowed to relax. There are dual pathways to enter the latter half of the reaction. The first pathway over the TS 3-1 (point (a) in Fig. 5) goes through a saddle point (e) nearly corresponding to the TS 3-2 via a shallow intermediate point (h) corresponding to the Int 3 of Fig. 3. The other pathway reaches a very low saddle point (f) corresponding to the TS 4-2, which is largely stabilized by the formation of the stable intermediate Int 4 of Fig. 3 (point (d) of Fig. 6). As seen from the PES, the two saddle points (e) and (f), and the two intermediate states (d) and (h) are almost completely continuous with only a negligible barrier less than 0.1 eV (the local maximum is located at the point (g)). Dynamically, it seems more likely that trajectories across the TS 3-1 in the path (a) fall down into the lower pathway, *i.e.* into the path (b), before crossing the 2nd transition state, TS 3-2, than the reverse transformation from the path (b) to the path (a). It must be noted that surpassing the TS 3-2 never affect the total reaction rate, since the rate-limiting step is at the 1st transition states.

Good continuity of the ER and LH pathways was confirmed over the wide region of the PES extending from the rate-limiting 1st transition states to the end of the reaction. However, it was concluded that the LH pathway starting from weakly trapped CO molecules at the Co^{2+} site was entropically much more favored in the rate-limiting N–N bond formation, and the subsequent N–O bond breakage was promoted by the attractive interaction of CO with the Co^{2+} site (Scheme 1).

5. Summary

To investigate the molecular-level mechanism of the NO reduction and adsorption promoted by CO molecules undetectable on the Co^{2+}-ensemble/γ-Al_2O_3 catalyst, we performed density functional theory calculations for the Co^{2+}-dimer/γ-Al_2O_3 catalyst. On the Co^{2+}-dimer model catalyst derived in the previous paper [20], three dinitrosyl adsorbates were found: two of them were conventional *gem*-dinitrosyl species (*gem*-dinitrosyl I and *gem*-dinitrosyl II) and the other was a *cis*-$(NO)_2$ dimeric species, where two NO molecules adsorbed at the adjacent Co^{2+} sites interacted with each other due to the opposed orientation of the unoccupied *d* orbitals on the adjacent two Co^{2+} ions. The vibrational frequencies of the *cis*-$(NO)_2$ dimer were almost identical to those of the *gem*-dinitrosyl species. The *gem*-dinitrosyl II, whose formation was accompanied with the Co^{2+}–O_{surf} bond scission, was considered to be the experimentally observed stable species, which was responsible for the spectator CO-promoted NO adsorption. We found that the reactivity of the *cis*-$(NO)_2$ dimer with CO was much higher than that of the geminal species since the *cis*-$(NO)_2$ dimer easily formed the N–N bond due to the $2\pi^*$–$2\pi^*$ hybridization between the adjacent NO species. The highly reactive *cis*-$(NO)_2$ dimer was able to react with unactivated gaseous or very weakly adsorbed CO molecules. In the most plausible mechanism, CO molecules are first very weakly trapped at the Co^{2+} sites in an undetectable manner, and then make a pseudo-compound intermediate with the *cis*-$(NO)_2$ dimer as a result of the rate-limiting N–N bond formation, which is readily converted to the gaseous $N_2O + CO_2$ products (Scheme 1). It is notable that there was a good continuity of the ER and LH pathways over the wide region of the PES extending from the rate-limiting 1st transition states to the end of the reaction. This study is the first to explain the high reactivity of a molecularly designed heterogeneous catalyst surface by the comprehensive and microscopic theoretical calculations comparing the experimental observations. The study also proves the significance of the molecular-level design of the active sites on catalyst surfaces by new insight of catalysis mechanisms to develop highly reactive catalysts.

Acknowledgments

The present study was supported by a Grant-in-aid for the 21st Century COE Program for Frontiers in Fundamental Chemistry from the Ministry of Education, Culture, Sports, Science and Technology. T.T. thanks JSPS for doctoral fellowship.

References

[1] Y. Iwasawa, Tailored Metal Catalysts, Reidel, Dordrecht, 1986.
[2] Y. Iwasawa, Characterization and chemical design of oxide surfaces, Stud. Surf. Sci. Catal. 101 (1996) 21–34.
[3] J.M. Thomas, R. Raja, G. Sankar, R.G. Bell, Molecular-sieve catalysts for the selective oxidation of linear alkanes by molecular oxygen, Nature 398 (1999) 227–230.
[4] Y. Iwasawa, Chemical design surfaces for active solid catalysts, Adv. Catal. 35 (1987) 187–264.
[5] M. Tada, Y. Iwasawa, Approaches to design of active structures by attaching and molecular imprinting of metal complexes on oxide surfaces, J. Mol. Catal. A: Chem. 204–205 (2003) 27–53.
[6] M. Tada, Y. Iwasawa, Advanced chemical design with supported metal complexes for selective catalysis, Chem. Commun. (2006) 2833–2844.
[7] Y. Iwasawa, Surface catalytic reactions assisted by gas phase molecules, Acc. Chem. Res. 30 (1997) 103–109.
[8] J.M. Thomas, R. Raja, D.W. Lewis, Single-site heterogeneous catalysts, Angew. Chem. Int. Ed. 44 (2005) 6456–6482.
[9] A.M. Argo, J.F. Odzak, F.S. Lai, B.C. Gates, Observation of ligand effects during alkene hydrogenation catalysed by supported metal clusters, Nature 415 (2002) 623–626.
[10] M. Tada, T. Taniike, L.M. Kantam, Y. Iwasawa, Chiral self-dimerization of vanadium complexes on a SiO_2 surface: the first heterogeneous catalyst for asymmetric 2-naphthol coupling, Chem. Commun. (2004) 2542–2543.
[11] R. Bal, M. Tada, T. Sasaki, Y. Iwasawa, Direct phenol synthesis by selective oxidation of benzene with molecular oxygen on an interstitial-N/Re cluster/zeolite catalyst, Angew. Chem. Int. Ed. 45 (2006) 448–452.
[12] A. Yamaguchi, K. Asakura, Y. Iwasawa, A new aspect of catalysis at designed surfaces: the role of gas phase molecules in surface catalytic reactions, J. Mol. Catal. A: Chem. 146 (1999) 65–76.
[13] T. Shido, A. Yamaguchi, K. Asakura, Y. Iwasawa, Surface catalytic reactions assisted by gas phase molecules: activation of reaction intermediates, J. Mol. Catal. A: Chem. 163 (2000) 67–77.
[14] A. Yamaguchi, T. Shido, K. Asakura, Y. Iwasawa, Surface catalytic reactions assisted by gas phase molecules on co-ensemble catalysts, Stud. Surf. Sci. Catal. 130 (2000) 605–610.
[15] M. Tada, T. Taniike, Y. Iwasawa, Understanding of novel surface events on a supported Co^{2+}-ensemble catalyst promoted by gas-phase molecules: increases in the amount and reactivity of adsorbed NO by CO undetectable at the catalyst surface, J. Phys. Chem. C 111 (2007) 11663–11675.
[16] Y. Iwasawa, M. Yamada, Y. Sato, H. Kuroda, Spectroscopic study on surface transformations of $Co_2(CO)_8$ supported on γ-Al_2O_3 or SiO_2, J. Mol. Catal. 23 (1984) 95–106.
[17] K. Asakura, Y. Iwasawa, Extended X-ray absorption fine structure studies on the structure change of the Al_2O_3-attached $[Co^{II}]_4$ catalyst during carbon monoxide oxidation reaction, J. Phys. Chem. 93 (1989) 4213–4218.
[18] D. Kaucký, A. Vondrová, J. Dědeček, B. Wichterlová, Activity of Co ion sites in ZSM-5, ferrierite, and mordenite in selective catalytic reduction of NO with methane, J. Catal. 194 (2000) 318–329.
[19] J. Dědeček, D. Kaucký, B. Wichterlová, Does density of cationic sites affect catalytic activity of Co zeolites in selective catalytic reduction of NO with methane? Top. Catal. 18 (2002) 283–290.
[20] T. Taniike, M. Tada, Y. Morikawa, T. Sasaki, Y. Iwasawa, Density functional theoretical calculations for a Co_2/γ-Al_2O_3 model catalyst: structures of the γ-Al_2O_3 bulk and surface and attachment sites for Co^{2+} ions, J. Phys. Chem. B 110 (2005) 4929–4936.
[21] T. Taniike, M. Tada, R. Coquet, Y. Morikawa, T. Sasaki, Y. Iwasawa, A new aspect of heterogeneous catalysis: highly reactive *cis*-$(NO)_2$ dimer and Eley–Rideal mechanism for NO–CO reaction on a Co-dimer/γ-alumina catalyst, Chem. Phys. Lett. 443 (2007) 66–70.

[22] J.K. Labanowski, J.W. Andzelm, Density Functional Methods in Chemistry, Springer-Verlag, New York, 1991.
[23] J.P. Perdew, K. Burke, M. Ernzerhof, Generalized gradient approximation made simple, Phys. Rev. Lett. 77 (1996) 3865–3868.
[24] B. Delley, An all-electron numerical method for solving the local density functional for polyatomic molecules, J. Chem. Phys. 92 (1990) 508–517.
[25] M. Dolg, U. Wedig, H. Stoll, H. Preuss, Energy-adjusted *ab initio* pseudopotentials for the first row transition elements, J. Chem. Phys. 86 (1987) 866–872.
[26] A. Bergner, M. Dolg, W. Kuechle, H. Stoll, H. Preuss, *Ab initio* energy-adjusted pseudopotentials for elements of groups 13–17, Mol. Phys. 80 (1993) 1431–1441.
[27] T.A. Halgren, W.N. Lipscomb, The synchronous-transit method for determining reaction pathways and locating molecular transition states, Chem. Phys. Lett. 49 (1977) 225–232.
[28] S.K. Park, V. Kurshev, C.W. Lee, L. Kevan, Electron spin resonance and optical spectroscopic studies of Co-ZSM-5 with nitric oxide, Appl. Magn. Reson. 19 (2000) 21–33.
[29] A. Rohrbach, J. Hafner, Molecular adsorption of NO on NiO(1 0 0): DFT and *DFT+U* calculations, Phys. Rev. B 71 (2005) 045405.
[30] M. Weinert, J.W. Davenport, Fractional occupations and density-functional energies and forces, Phys. Rev. B 45 (1992) 13709–13712.
[31] G. Kresse, A. Gil, P. Sautet, Significance of single-electron energies for the description of CO on Pt(1 1 1), Phys. Rev. B 68 (2003) 073401.
[32] K. Doll, CO adsorption on the Pt(1 1 1) surface: a comparison of a gradient corrected functional and a hybrid functional, Surf. Sci. 573 (2004) 464–473.
[33] A. Rohrbach, J. Hafner, G. Kresse, Molecular adsorption on the surface of strongly correlated transition-metal oxides: a case study for CO/NiO(1 0 0), Phys. Rev. B 69 (2004) 075413.
[34] G. Pacchioni, C.D. Valentin, D. Dominguez-Ariza, F. Illas, T. Bredow, T. Klüner, V. Staemmler, Bonding of NH_3, CO, and NO to NiO and Ni-doped MgO: a problem for density functional theory, J. Phys.: Condens. Matter 16 (2004) S2497–S2507.
[35] P.P. Rushton, S.J. Clark, D.J. Tozer, Density-functional calculations of semiconductor properties using a semiempirical exchange–correlation functional, Phys. Rev. B 63 (2001) 115206.
[36] B. Hammer, J.K. Nørskov, Adsorbate reorganization at steps: NO on Pd(2 1 1), Phys. Rev. Lett. 79 (1997) 4441–4444.
[37] A. Bogicevic, K.C. Hass, NO pairing and transformation to N_2O on Cu(1 1 1) and Pt(1 1 1) from first principles, Surf. Sci. 506 (2002) L237–L242.
[38] G. Kresse, J. Hafner, *Ab initio* molecular dynamics for liquid metals, Phys. Rev. B 47 (1993) 558–561.
[39] S.L. Dudarev, G.A. Botton, S.Y. Savrasov, C.J. Humphreys, A.P. Sutton, Electron-energy-loss spectra and the structural stability of nickel oxide: An LSDA+U study, Phys. Rev. B 57 (1998) 1505–1507.
[40] P.E. Blöchl, Projector augmented-wave method, Phys. Rev. B 50 (1994) 17953–17979.
[41] K. Nakanishi, P.H. Solomon, Infrared Adsorption Spectroscopy, Holden-Day, San Francisco, 1977.
[42] F. Garin, Mechanism of NO_x decomposition, Appl. Catal. A: Gen. 222 (2001) 183–219.
[43] G. Centi, S. Perathoner, Nature of active species in copper-based catalysts and their chemistry of transformation of nitrogen oxides, Appl. Catal. A: Gen. 132 (1995) 179–259.
[44] K. Hadjiivanov, B. Tsyntsarski, T. Nikolova, Stability and reactivity of the nitrogen-oxo species formed after NO adsorption and $NO + O_2$ coadsorption on Co-ZSM-5: an FTIR spectroscopic study, Phys. Chem. Chem. Phys. 1 (1999) 4521–4528.
[45] C.E. Dinerman, G.E. Ewing, Infrared spectrum, structure, and heat of formation of gaseous $(NO)_2$, J. Chem. Phys. 53 (1970) 626–631.
[46] C.M. Western, P.R.R. Langridge-Smith, B.J. Howard, S.E. Novick, Molecular beam electric resonance spectroscopy of the nitric oxide dimer, Mol. Phys. 44 (1981) 145–160.
[47] M.P. Jigato, D.A. King, A. Yoshimori, The chemisorption of spin polarised NO on Ag{1 1 1}, Chem. Phys. Lett. 300 (1999) 639–644.
[48] Z.P. Liu, S.J. Jenkins, D.A. King, Why is silver catalytically active for NO reduction? A unique pathway via an inverted $(NO)_2$ dimer, J. Am. Chem. Soc. 126 (2004) 7336–7340.
[49] R. Burch, S.T. Daniells, P. Hu, The mechanism of N_2O formation via the $(NO)_2$ dimer: a density functional theory study, J. Chem. Phys. 121 (2004) 2737–2745.
[50] T.R. Ward, R. Hoffmann, M. Shelef, Coupling nitrosyls as the first step in the reduction of NO on metal surfaces: the special role of rhodium, Surf. Sci. 289 (1993) 85–99.
[51] J.K. Park, H. Sun, Relative stabilities of $(NO)_2$, Chem. Phys. 263 (2001) 61–68.